RSC Advances

ROYAL SOCIETY OF CHEMISTRY

www.rsc.org/advances

RSC Advances

RSCPublishing

ARTICLE

Mesoporous TiO_2 microbead electrodes for solid state dye-sensitized solar cells

Cite this: DOI: 10.1039/x0xx00000x

M. Pazoki,[a] J. Oscarsson,[b] L. Yang,[c] B.W. Park,[a] E. M.J. Johansson,[a] H. Rensmo,[b] A. Hagfeldt[a] and G. Boschloo[a]

Received 00th January 2012,
Accepted 00th January 2012

DOI: 10.1039/x0xx00000x

www.rsc.org/

Mesoporous TiO_2 microbead films have been investigated as working electrode for solid state dye sensitized solar cells and 3.5% efficiency was achieved for 4 micrometer thick films under 1 sun illumination. Compared to conventional mesoporous solar cells, microbead films have higher porosity, increased open circuit voltage, lower fill factor and current density, faster transport time and lower electron lifetime. Cross sectional scanning electron microscopy results show that the pore filling of a solid hole conductor (spiro-OMeTAD) inside the entire mesoporous bead film is very good even for 4 micrometer thick films. The high porosity of the microbead film allows good penetration of spiro in thick films, while its high surface area ensures good dye coverage. X-ray photoelectron spectroscopy data reveal lower density of intra-bandgap trap states for microbead films compared to conventional mesoporous TiO_2 films, which could be in part responsible for faster transport of electrons and higher voltage in microbead films. Optimization of microbead films for solid state dye sensitized solar cells can be an interesting possibility for highly efficient and relatively thick film solid state solar cells.

Introduction

Dye sensitized solar cells (DSCs) were introduced in 1991 by Michael Grätzel as a low cost and environmentally friendly molecular device among novel thin film solar cells.[1] During the last two decades, a lot of research has been done for understanding the interfacial processes in the DSC, increasing the efficiency and stability, decreasing the cost and to promote commercialization of the DSCs.[2-4] Solid state DSCs (SSDSCs) replaced the volatile liquid electrolyte of the traditional DSCs with a solid hole conductor in which the hole-conductance is performed by hole-hopping between hole conductor molecules.[5] The most efficient SSDSCs up to now have a certified efficiency of 6.1 % using the small molecule hole conductor 2,2',7,7'-tetrakis(N,N-dimethoxyphenylamine)-9,9'-spirobifluorene (spiro-OMeTAD) along with the organic sensitizer C220 with high extinction coefficient.[6] Doping of solid state hole conductors and its effect on the solar cell performance has been investigated by several groups[7] and an efficiency of 7.2% has been reported by Grätzel using a cobalt complex as dopant for spiro-OMeTAD.[8]

Incomplete pore filling and high back recombination rates are the two most important issues for the SSDSCs efficiency, which limits the thickness of the TiO_2 film.[9-11] Using new morphologies in the SSDSCs can enhance the pore filling and give faster charge transport in these cells.[12-14] Different one-dimensional structures have been introduced for the SSDSCs to improve the pore filling and electronic transport. Chen et al used TiO_2 nanotubes in the SSDSC achieving 1.7% efficiency under 1 sun light intensity.[15] Wang et al. have used ordered TiO_2 nanorods in SSDSCs with 2.9 % efficiency under 1 sun light intensity.[13] Better pore filling in one dimensional structures leads to higher optimum thickness of nanorod and nanotube based SSDSCs compared to mesoporous nanoparticulate SSDSCs. Due to their lower surface area usually the efficiency is less than 3%. Snaith et al. reported a new single crystalline mesoporous structure with 3.1 % efficiency having faster transport time and lower lifetime compared to standard SSDSCs.[14] Engineering of the interface between TiO_2 and hole transport material can reduce the charge recombination in SSDSCs.[16]

According to the multiple trapping model, [17] electron transport inside the mesoporous TiO_2 films depends strongly on the number of traps regardless of dimensionality of the embedded nanostructure. Snaith et al reports on the effect of the crystallite size on the electron diffusion coefficient in block co-polymer films.[18]

Mesoporous microbeads have been used in liquid dye sensitized solar cells as efficient structure with high film porosity, light harvesting efficiency and fast electronic diffusion.[19-21] Efficiencies of more than 10% are achievable by a one step screen printing of microbead paste in liquid based DSCs.[19] In this paper, we are using the microbead structures for SSDSCs. Higher electron diffusion coefficient and big interparticle holes in the microbead films can be interesting for better pore filling and charge transport in the SSDSCs, allowing us to have thicker films. Also higher diffuse light scattering and surface

area in the microbead films compared to standard nano-particulate films can enhance the light harvesting efficiency of the SSDSC. Here we have fabricated devices of microbead films and compared them to standard Dyesol paste films regarding the photo-chemical behavior of two devices.

Experimental

Synthesis of microbeads: Mesoporous microbeads were synthesized according to the work of Dehong Chen et al.[17] In summary, 7.95 g hexadecylamine was dissolved in 800 mL Ethanol and 3.2 mL 0.1 M KCl in De-ionized (DI) water was added to the solution. 18.1 mL of titanium isoproxide (TIP) was then added to the solution at room temperature under high stirring conditions. The milky solution was kept in room temperature for 18 hours and then centrifuged, dried and moved to the Teflon autoclave with water, ethanol and 0.4 mM ammonia solution (for each 1.6 gram of TiO_2 powder, 20 mL ethanol and 10 mL DI water). The autoclave was kept at 165 °C for 12 hours and the final product was used for making the microbead paste according to the procedure of Ito et al.[22] Scanning and tunneling electron microscopy (SEM & TEM), X-ray diffraction (XRD) and X-ray photoemission spectroscopy (XPS) were used to characterize the microbead films.

Photoelectron Spectroscopy (PES:) PES measurements with photon energies 150 eV and 758 eV were performed at the undulator beamline I411 at the Swedish national synchrotron facility MAX-IV in Lund, Sweden.[23] The electron take off angle was 70˚. Kinetic energies of the ejected photoelectrons were measured using a Scienta R4000 WAL analyzer. Measurements with the photon energy 1487 eV (Al Kα) were done using an in-house ESCA300 setup. The electron take off angle was 90˚. Measurements with photon energies 4000 eV and 6000 eV were performed at the HIKE end station at the KMC-1 beamline at BESSY II at Helmholtz Zentrum Berlin, Germany.[24] The end station utilizes a Scienta R4000 analyzer and the electron take off angle was 85˚. Varying the photon energy corresponds to varying surface sensitivity of the measurement. Higher photon energy leads to higher bulk sensitivity and, correspondingly, lower photon energy gives higher surface sensitivity since the inelastic mean-free path of ejected photoelectrons increase with increasing photon energy.

All measured data was energy calibrated versus the $Ti2p_{3/2}$ peak that was set to a binding energy of 458.56 eV.[25] XPS has primarily been used to study the Ti 2p core level and the valence band of the films. Other core levels as O1s and C1s were also measured to study possible surface contamination.

Device Fabrication: Fluorine doped SnO_2 coated glass (FTO) was pre-cut from the non-conductive side (electrode dimension = 1.2 × 2.4 cm), partly etched (etched area of 4 mm X 24 mm) by zinc powder and 2M HCl in water and cleaned with detergent, DI water, 0.1M HCl in ethanol, acetone and ethanol. For each cleaning step the electrodes were kept in ultrasonic bath for 30 minutes and finally rinsed with DI water. A flat and dense TiO_2 underlayer was coated on the FTO by spray pyrolysis in 450 ˚C for 5 cycles. Between each cycle, 30 seconds waiting time was necessary to complete the reaction. The precursor consists of 5.68 g TIP, 20.02 g acetylacetone diluted by 100 mL isopropanol. The electrodes were cooled down to room temperature according to the following program: 450 °C (20 minutes)-> 350 °C (20 minutes)->250 °C (20 minutes)-> room temperature.

The standard TiO_2 mesoporous layer was deposited on the working electrode by spin coating (2400 RPM for 30 seconds) of TiO_2 paste (29:29:42 weight ratio of ethanol, terpineol and Dyesol DSL18R paste) and dried on 70 ˚C hotplate for 20 minutes. The sintering program of the working electrode in the cubic furnace is 280 ˚C (15 minutes), 350 ˚C (15 minutes), 420 ˚C (15 minutes) and 500 ˚C (30 minutes) with a ramp of 3.5 °C per minute between the steps. The microbead films were deposited on the electrode using the doctorblade method and dried on a 50 °C hotplate for 1 hour. The microbead electrodes were kept at 450 ˚C for half an hour for sintering (ramp 1.5 °C per minute). Thickness of the films was measured by a Dektak profilometer. $TiCl_4$ treatment of the films were done in 50 mL of 0.2 mM $TiCl_4$ solution in deionized water in 70 ˚C for 30 minutes with subsequent sintering in 450 ˚C for 30 minutes.

Working electrodes were immersed in the dye bath (LEG4 from Dyenamo AB) (Fig. S.1 of supporting information) 0.2 mM in acetonitrile : tert-butanol (1:1 volumetric ratio)) when the electrodes had cooled down to 80 ˚C and kept in the dye bath overnight. The electrodes were then rinsed using acetonitrile and dried in vacuum (Fig. S.2 of supporting information shows the typical dyed microbead working electrode). The hole conductor Spiro-OMeTAD (Fig. S.1 of supporting information) solution was spin coated onto the dyed films (2000 RPM, 30 seconds, waiting time 1 minute). The hole conductor solution contained 150 mM spiro-OMeTAD (spiro), 120 mM 4TBP and 20 mM LiTFSI ($LiN(CF_3SO_2)_2$) in chlorobenzene which was prepared in a glove box. The concentration of LiTFSI is changed for some of the samples mentioned in the results and discussions. Then the FTO part of the electrode was cleaned by chlorobenzene and then covered by a silver contact (200 nm thick) by thermal vacuum evaporation. Dye deloading of the films was done by putting the dyed films in 5 ml of 0.1 M tetrabutylammonium hydroxide in solution of (9:1 volumetric ratio of methanol : ethanol) and the final solution was measured by UV-vis spectroscopy.

Device Characterization : The number of adsorbed dye molecules was estimated by dye desorption, calculated according to $A=\varepsilon Cl$, in which A is the optical absorbance of the deloading solution, ε is the extinction coefficient of the dye, l is the optical path length (1 cm) and C is the concentration of the dye in the solution.[26]

The solar simulator model 91160-Newport along with a Keithley 2400 source meter was used for measuring the efficiency of the solar cells. A 0.126 cm^2 black mask was used for measuring the photon to current efficiency (PCE) of the cells under 100 mW cm^{-2} AM1.5G light. Internal photon to current efficiency (IPCE) spectra of the SSDSCs was measured using a homemade setup consisting of a Xenon lamp (Spectral

Products ASBXE- 175), a monochromator (Spectral products CM110), a calibration silicon diode (Thorlabs LM1RM), a multimeter (Keithley model 2700) to read the current of the solar cell by measuring the voltage over a series-connected 100 ohm resistor.

Electron lifetime and transport time were measured using small perturbation square wave modulated light, measuring transient photocurrent and photo-voltage in the homemade Toolbox setup. The light was generated by a LED (Luxeon-Lumiled) and its intensity was modulated by a wave generator with different bias potentials and the current/potential was collected by a low noise current preamplifier (Stanford research system-model SR570) connected to PC by data acquisition board (DAQ- National Instrument BVC-2110).

Results and Discussions

Fig. 1 shows SEM and TEM images of the microbead films. Each bead is around 900 nm in diameter and composed of small nanoparticles. The microbeads possess high surface area (S_{BET} ~ 110 m^2g^{-1})[21] and have high light scattering properties.[16] Furthermore, microbead films has large pores in between the beads, that are expected to improve the infiltration with solid molecular hole conductors. The high crystallinity of the nanoparticles is demonstrated by TEM, see Fig. 1c and d. The crystal planes of anatase TiO_2 are observed in the TEM, and it is found that each nanoparticle with a size around 14 nm is single crystalline. Using the ammonium in the solvothermal synthesis causes the elongation of single crystal in the 101 direction (Fig. 1c and 1d). The XRD pattern (Fig. S3 of supporting information) confirms anatase crystalline phase of microbead film with 14 nm crystallite size according to Debye-Scherrer formula, which is in agreement with TEM data.

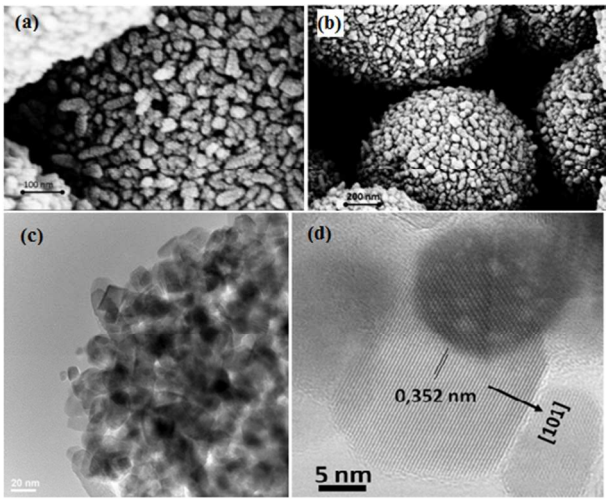

Fig. 1. SEM (a, b) and TEM images (c, d) of the synthesized TiO_2 anatase mesoporous microbeads and their crystallites.

Fig. 2 shows the SEM cross section images of fabricated solar cells for microbead based (MB) and Dyesol paste based (DSL) SSDSCs. TiO_2 blocking layer, mesoporous TiO_2/dye/hole conductor layer, hole conductor capping layer and silver back contacts can be seen in Fig. 2. The optimized thickness of the TiO_2 layer was 3.9 μm for MB and 2.4 μm for DSL devices, respectively. MB films with higher thickness and / or porosity do not possess a complete capping layer of spiro-OMeTAD, resulting in poor device performance. Compared to standard mesoporous TiO_2 films, the higher surface roughness of MB films causes the silver contact to have the same shape and roughness as the MB film itself. The pore filling by spiro-OMeTAD in both types of films seems complete, down to the blocking TiO_2 layer, as observed from Fig. 2. Pores are, however, not expected to be 100% filled. The large pores inside the MB films allow for a good pore filling inside thicker films up to 4 micron.

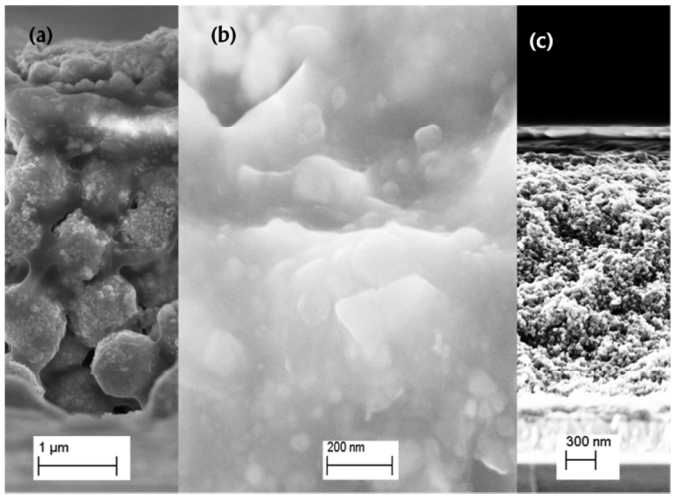

Fig. 2. SEM cross sectional images of fabricated devices: a) MB and c) DSL. b) Complete coverage of hole conductor on the surface of an individual microbead particle.

Fig. 3 and Table 1 show the photovoltaic properties of fabricated SSDSCs with LEG4 organic dye and spiro-OMeTAD as hole conductor. A promising 3.5% efficiency was achieved by the microbead films (MB-SSDSC), which is lower than the 5.85% efficiency of standard films (DSL-SSDSC), but in the best of our knowledge is the highest efficiency reported for morphologies other than standard nanoparticles. The reported efficiency is for the champion device and statistics of the device efficiency for all fabricated cells is reported in section S.III of supporting information. MB-SSDSC has a higher open circuit voltage (V_{oc}), lower short circuit current density (J_{sc}) and fill factor (FF) compared to DSL-SSDSC. Both devices show linear J_{sc} versus light intensity (Fig. S4 of supporting information). The amount of dye on these electrodes, determined by a dye desorption study, are 8.7×10^{-4} mol cm^{-3} for DSL and 7.1×10^{-4} mol cm^{-3} for MB . The total number of dye molecules on the MB is higher because of higher thickness of the TiO_2 active layer. Normalization with respect to the thickness shows that DSL adsorbs 19 % more dye, which may be explained by the presence of large pores in the MB films. Current voltage fittings to data of Fig. 3 reveals

that rough surface of the microbead film can cause additional contact resistance for the MB device and decreases the fill factor of the device (Fig. S8 of supporting information).

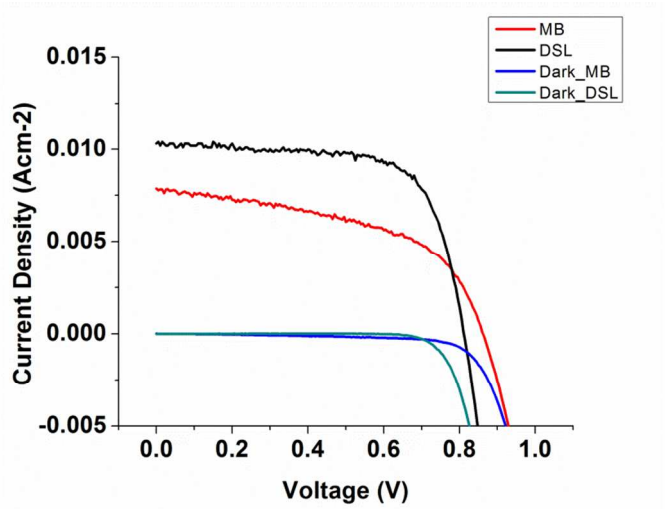

Fig. 3. Current-voltage curves for the MB-SSDSC and DSL-SSDSC devices under 1 sun illumination at in the dark.

Table 1. Solar cell characteristics of the fabricated devices under 1 sun light intensity.

Device	Efficiency [%]	Voc [mV]	Jsc [mA cm^{-2}]	Fill factor [%]	Are [cm
MB-SSDSC	3.51	860	7.88	51.9	0.126
DSL-SSDSC	5.84	810	10.3	69.9	0.126

IPCE spectra of the fabricated cells are shown in Fig. 4. The microbead films show lower IPCE than the DSL films, which is in accordance with the current – voltage data in Fig. 3. A dip at about 520 nm in the IPCE spectra is related to absorption by oxidized spiro-OMeTAD.[7] The normalized IPCE of MB shows no significant broadening compared to DSL, probably because of the presence of a highly scattering silver back contact, which acts as a mirror to reflect back the photons and increase the light harvesting of the transparent DSL layer. Theoretical calculations show that in most of the cases for devices with different diffusion length and device thickness, the back scattering layer is more effective than internal scattering for light harvesting efficiency of the device which is in qualitative agreement with our data.[27]

Changing the lithium salt concentration did not show improved performance for any of the devices (Fig. S5 of supporting information). For the MB device, V_{oc} decreases and FF increases with increasing the Li concentration in the spiro-OMeTAD solution and the Jsc has a peak near the optimized Li concentration, which is in agreement with previous reports about standard DSL based solid state DSCs.[28]

Fig. 5 shows electron lifetime and transport time of the fabricated devices. Transport time of electrons is faster in the MB device. Superior transport time and diffusion coefficient of MB structure compared to ordinary nanoparticles in liquid based DSCs has been reported previously.[19-20] MB-based devices have shorter electron lifetimes compared to DSL-based devices. Higher surface area of microbead particles compared to Dyesol paste can explain the lower lifetime of the MB device. These data are in agreement with liquid based DSCs reported elsewhere.[19-20] The Fermi level in short circuit conditions is at least 100-200 meV lower than open circuit voltage conditions.[29] Electron lifetime measurements indicate that the lifetime in short circuit conditions is more than 10 ms, which is sufficiently long to not affect the transport time data values.

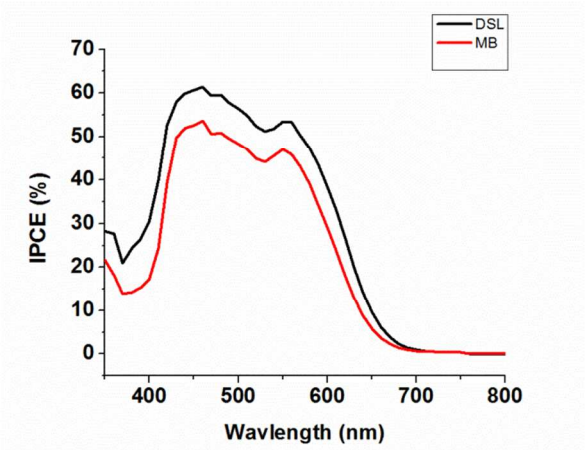

Fig. 4. IPCE spectra of the MB-SSDSC and DSL-SSDSC devices.

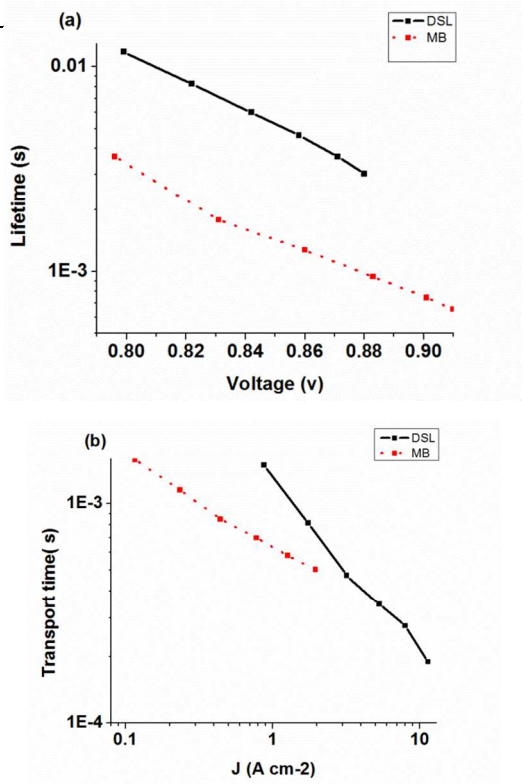

Fig. 5. a) Electron lifetime and b) transport time of fabricated devices

From the lower trap density of the MB film (see Fig. 6) one may expect the MB device to have lower charge than the DSL device at the same potential. This should contribute to a lower recombination and a lower dark current for the MB device in the dark conditions (Fig. 3). But during illumination there are further recombination routes for electrons such as reduction of the oxidized dye or oxidized spiro. Incomplete spiro pore filling inside single microbead particles (which increases recombination to oxidized dyes) can be a possible explanation for the lower lifetime of the illuminated MB device. Studies of charge-potential graphs can be useful for further investigation of lifetime in MB devices.

Fig. S6a shows the Ti 2p core level of the DSL and MB films measured with different photon energies. Ti^{3+} is expected at about 2 eV lower binding energy than Ti^{4+} observed at 458.56 eV. In all spectra we observe that the Ti^{3+} amount is minor. To highlight this further, the spectra have been normalized at the Ti $2p_{3/2}$ peak for comparison. The relation between Ti^{4+} and Ti^{3+} in the films does not change when changing the probing depth (photon energy) of the measurement.[23] This indicates that the TiO_2 films are equal in the bulk and at the surface; hence the amount of surface defects is low in both DSL and MB.

Fig. S5b shows the valence band of the films measured with higher photon energies (1487 – 6000 eV). There are no significant differences between DSL and MB at each photon energy correspondingly. Fig. 6 shows the outermost part of the valence band measured with a photon energy of 150 eV. The spectra reveals occupied electronic states in the band gap, i.e. below the valence band edge. This structure is often referred to as trap states and comes from electrons that are trapped in the band gap due to imperfections in the structure and particle neckings. The spectra are intensity normalized and energy referenced to the Ti 3p core-level and the DSL film shows a significantly higher amount of trapped electrons compared to the MB film. Thus, there are more trap states in DSL than in MB.

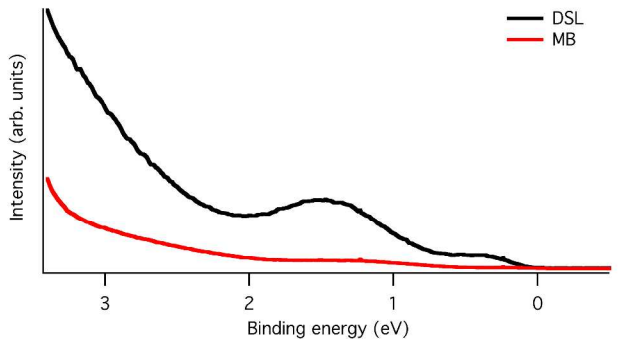

Fig. 6. The outermost part of the valence band revealing trap states in the band gap. Measured with a photon energy of 150 eV.

In a first approximation, the higher the density of trap states, the longer time it takes to fill them. This means that more electrons get trapped and thus the electron transport time increases and the voltage output decreases. A low trap state density corresponds then to faster electron transport and higher voltage. This is often called the multiple-trapping model.[17] This behaviour agrees well with the measurements presented in Fig. 5. This is furthermore confirmed by calculating the trap depth in the films (see Table S1 and Fig. S7 in Supporting Information). Not presented here are the measurements of the C1s core level. A small amount of carbon was found on all of the samples. This is expected since the samples are prepared ex-situ. However, the amount was sufficiently low to not affect the results.

Conclusions

Mesoporous microbeads were applied as TiO_2 active film for solid state dye sensitized solar cells and 3.5% efficiency was achieved under AM 1.5 conditions. The lower amount of trap states can explain in part the faster electron transfer and the higher voltage of MB compared to DSL based SSDSCs. Lifetime and transport time data –were similar to liquid based DSCs- show lower lifetime and faster transport time for the MB DSC compared to DSL DSC. The presence of a reflective silver back contact makes that the light scattering properties of MB cells are of less importance. Microbead electrodes are good candidates for anodes in efficient SSDSC solar cells.

Acknowledgements

The Swedish Energy Agency, the Swedish Research Council (VR) and the European Community's Seventh Framework Program (SANS, FP / 2007-2013 under Grant Agreement No. 226716) are appreciated for funding the project. We acknowledge Helmholtz Zentrum Berlin, BESSY II for provision of synchrotron radiation at beamline KMC-1 and especially thank Mihaela Gorgoi for all the support at the beamline. We also thank the staff at MAX-IV for assistance, support and a friendly working atmosphere. We thank Azhar Zia for help and discussions of the XPS data.

Notes and references

[a] Department of Chemistry Ångström Laboratory, Physical Chemistry, Uppsala University, Box 523, SE-75120, Uppsala, Sweden.
[b] Department of Physics and Astronomy, Molecular and Condensed Matter Physics, Uppsala University, Box 516, SE-75120, Uppsala, Sweden..

Electronic Supplementary Information (ESI) available: [details of any supplementary information available should be included here]. See DOI: 10.1039/b000000x/

1 B. O'Regan and M. Gratzel, *Nature,* 1991, **353**, 737.
2 A. Hagfeldt, G. Boschloo, L. Sun,L. Kloo, and H. Pettersson, *Chem. Rev.,* 2010 , **110**, 6595.

3 J. B. Baxter, *Journal of vacuum and technology A*, 2012, **30**, 020801.
4 N. T.etreault and M. Gratzel, *Energy Environ. Sci.*, 2012, **5**, 8506.
5 U. Bach, D. Lupo, P. Comte, J. E. Moser, F.Weissortel, J. Salbeck, H. Spreitzer and M. Gratzel, *Nature,* 1998, **395**, 583; H. J. Snaith and L. S. Mende *Adv. Mater.,* 2007, **19**, 3187.
6 N.Cai, S. J. Moon, L. Cevey-Ha, T.Moehl, R. Humphry-Baker, P.Wang, S.M. Zakeeruddin, M. Gratzel, *Nano Lett,.* 2011, **11**, 1452.
7 A.Abate, D.Hollman, J.Teuscher, S.Pathak, R.Avolio, G.D'Errico, G.Vitelio, S. Fantacci, H.J.Snaith, *J. Am. Chem. Soc.,* 2013, **135**, 13538; U. B. Cappel, T. Daeneke, and U. Bach, *Nanoletters,* 2012, **12**, 4925; L. Yang, B. Xu, D. Bi, H. Tian, G. Boschloo, L. Sun, A. Hagfeldt, and E. M. J. Johansson, *J. Am. Chem. Soc.,* ,2013, **135**,7378.; R. Scholin, M. H. Karlsson, S. K. Eriksson, H. Siegbahn, E. M. J. Johansson, H. Rensmo, *J. Phys. Chem. C.* 2012, **116**, 50, 26300.
8 J. Burschka, A. Dualeh, F. Kessler, E. Baranoff, N. Cevey-Ha, C. Yi, M. K. Nazeeruddin, and M. Gratzel, *J. Am. Chem. Soc.,* 2011, **133**, 18042.
9 H. J. Snaith, R. Humphry-Baker, P. Chen, I. Cesar, S. M. Zakeeruddin and M. Gratzel, *Nanotechnology,* 2008 ,**19**, 424003.
10 J. Melas-Kyriazi, I.K. Ding, A. Marchioro, A. Punzi, B. E. Hardin, G. F. Burkhard, N. Tétreault, M. Grätzel, J.E. Moser, and M. D. McGehee, *Adv. Energy Mater*., 2011, **1**, 407.
11 P.Docanpo, A.Hey, R.Gunning, H.J.Snaith, S. Guldin and U. steiner *Adv. Func. Mater.,* 2012, **22**, 5010.
12 P. Chen, J. Brillet, H. Bala, P. Wang, S. M. Zakeeruddin and M. Grätzel, J. Mater. Chem., 2009**,19**, 5325.
13 M. Wang, J. Bai, F. L.Formal, S. Moon, L. Cevey-Ha, R. Humphry-Baker, C. Grätzel, S. M. Zakeeruddin, and M. Grätzel, *J. Phys. Chem. C,* 2012, **116**, 3266.
14 E. J. W. Crossland, N. Noel, V. Sivaram, T. Leijtens, J. A. Alexander-Webber and H. J. Snaith, *nature letters*, 2013, **494**, 215.
15 D. Chen, L. Cao, F. Huang, P. Imperia, Y. Cheng, and R. A. Caruso, *J. Am. Chem. Soc,.* 2010, **132**,4438.
16 B.R.Hardin, H.J.Snaith,; M.D.McGehee, *nature photonics,* 2012, **6**, 162.
17 J. Nelson, *Phys. Rev. B,.* 1999**, 59**,15374.
18 P. Docampo, S. Guldin, U. Steiner, and H. J. Snaith, *J. Phys. Chem. Lett,.* 2013, **4**, 698.
19 F. Sauvage, D. Chen, P. Comte, F. Huang,_ L. Heiniger, Y. Cheng, R. A. Caruso, and M. Graetzel, *ACS Nano,* 2010, **4**, 4420.
20 M. Pazoki, N. Taghavinia, A. Hagfeldt and G. Boschloo, *J. Phys. Chem. C.,* 2014 doi:10.1021/jp4113574 ; M. Pazoki, *P.h.D Thesis*, Sharif university of Technology, December, 2012.
21 D. Chen, F. Huang, Y. Cheng, and R. A. Caruso , *Adv. Mater.,* 2009, **21**, 2206.
22 S. Ito, P. Chen, P. Comte, M. K. Nazeeruddin, P. Liska, P. Pechy and M. Gratzel, *Prog. Photovolt: Res. Appl.,* 2007**, 15**,603.
23 M. Bassler, J.O.Forsell, O.Björneholm, R.Feifel, M.Jurvansuu, S.Aksela, S.Sundin, S.L.Sorensen, R.Nyholm, A.Ausmees, *J. Electron Spectrosc,.* 1999, **953**,101.
24 M. Gorgoi, S.Svensson, F.Schäfers, G.Öhrwall, M.Mertin, P.Bressler, O.Karis, H. Siegbahn, A.Sandell, H.Rensmo, *Nucl. Instrum. Meth. A,,* 2009, **601**, 45.
25 E.M.J. Johansson, M.Hedlund, H.Siegbahn, H.Rensmo, *J. Phys. Chem. B*, 2005, **109**, 22256.
26 S.Ardo, And G.J. Meyer, *J. Am. Chem. Soc.,* 2011, **133**, 15384.
27 F.E. Galvez, E. Kemppainen, H. Miguez and J. Halme, *J. Phys. Chem. C*, **116**, 11426.
28 A. Abate, T. Leijtens, S. Pathak, J. Teuscher, R. Avolio, M. E. Errico, J. Kirkpatrik, J. M. Ball, P. Docampo, I. McPherson and H. J. Snaith, *Phys. Chem. Chem. Phys.*, 2013,**15**, 2572.
29 G. Boschloo, A. Hagfeldt, *J. Phys. Chem. B,* 2005, ***109***, 12093.

